Energy 36 (2011) 3406–3418

Contents lists available at ScienceDirect

Energy

journal homepage: www.elsevier.com/locate/energy

Study of working fluid selection of organic Rankine cycle (ORC) for engine waste heat recovery

E.H. Wang [a], H.G. Zhang [a,*], B.Y. Fan [a], M.G. Ouyang [b], Y. Zhao [c], Q.H. Mu [c]

[a] College of Environmental and Energy Engineering, Beijing University of Technology, Pingleyuan No. 100, 100124 Beijing, China
[b] State Key Laboratory of Automotive Safety and Energy, Tsinghua University, Qinghuayuan, 100084 Beijing, China
[c] Institute of Mechanics, Chinese Academy of Sciences, Beisihuanxi Road No. 15, 100190 Beijing, China

ARTICLE INFO

Article history:
Received 16 August 2010
Received in revised form
14 March 2011
Accepted 15 March 2011
Available online 21 April 2011

Keywords:
Organic Rankine cycle
Waste heat recovery
Working fluid
Engine
Matlab

ABSTRACT

Organic Rankine Cycle (ORC) could be used to recover low-grade waste heat. When a vehicle is running, the engine exhaust gas states have a wide range of variance. Defining the operational conditions of the ORC that achieve the maximum utilization of waste heat is important. In this paper the performance of different working fluids operating in specific regions was analyzed using a thermodynamic model built in Matlab together with REFPROP. Nine different pure organic working fluids were selected according to their physical and chemical properties. The results were compared in the regions when net power outputs were fixed at 10 kW. Safety levels and environmental impacts were also evaluated. The outcomes indicate that R11, R141b, R113 and R123 manifest slightly higher thermodynamic performances than the others; however, R245fa and R245ca are the most environment-friendly working fluids for engine waste heat-recovery applications. The optimal control principle of ORC under the transient process is discussed based on the analytical results.

1. Introduction

Only 30% of an engine's fuel combustion energy is converted into useful work to drive a vehicle and its accessory loads. The remainder is engine waste heat dissipated by the engine exhaust system, coolant system, and convection as well as radiation from the engine block. Nearly 40% of heat energy is wasted with the engine exhaust gas [1]. If this portion of waste heat could be harnessed, energy efficiency will be enhanced, where vehicles all over the world could save lots of energy. Furthermore, global warming will be decreased.

Organic Rankine Cycle (ORC) could be used to recover low-grade waste heat from engine exhaust gas. The advantages of ORC compared with other heat engine cycles are outstanding. First, high waste energy utilization is achieved by ORC when compared with other waste heat-recovery approaches. Next, it is easy to downsize system volume and weight, which is rigid for vehicle applications. Finally, the cost of ORC is cheaper than others such as a thermoelectric generator.

Many investigations about ORC were carried out and can be classified into three main categories according to their application domains. The first is geothermal energy utilization. Hettiarachchi et al. [2] evaluated optimum cycle performance when evaporation and condensation temperatures, and geothermal and cooling water velocities were varied, and then compared the results to working fluids that included ammonia, HCFC-123, n-Pentane, and PF5050. Saleh et al. [3] investigated 31 pure component working fluids for sub-critical and supercritical ORCs for geothermal power plants. The second category reviewed is solar energy harnessing. Yamamoto et al. [4] estimated the optimum operating conditions of ORC comparing HCFC-123 and water as working fluids. Tchanche et al. [5] comparatively accessed 20 working fluids for use in low-temperature solar organic Rankine cycle systems. The final category considered is low-grade waste heat recovery. Hung et al. [6] analyzed ORC efficiency using cryogens such as benzene, ammonia, R11, R12, R134a and R113 as working fluids. Maizza and Maizza [7] investigated the thermodynamic and physical properties of 20 unconventional fluids used in organic Rankine cycles supplied by waste energy sources. Liu et al. [8] reviewed the effects of 10 various working fluids on the thermal and total heat-recovery efficiencies of the organic Rankine cycle. Wei et al. [9,10] analyzed system performance and optimized the working conditions of an ORC using R245fa when a simulation of a dynamic model was conducted in Dymola [11]. Drescher and Bruggemann [12] developed software to find thermodynamically suitable fluids for ORC in biomass power and heat plants. Mago et al. [13] analyzed a regenerative ORC using four dry organic fluids to

* Corresponding author. Tel./fax: +86 10 6739 2914.
E-mail address: zhanghongguang@bjut.edu.cn (H.G. Zhang).

0360-5442/$ – see front matter © 2011 Elsevier Ltd. All rights reserved.
doi:10.1016/j.energy.2011.03.041

convert waste energy to power from low-grade heat sources. Lemort et al. [14] studied ORC system performance with a scroll expander instead of a turbine with R123 as the working fluid. Dai et al. [15] adopted a genetic algorithm to optimize the working conditions of ORC and compared 10 working fluids for low-grade waste heat recovery. Angelino and Colonna di Paliano [16] evaluated organic-fluid mixtures as working media for Rankine power cycles. Chen et al. [17] compared a carbon dioxide, trans-critical power cycle with an organic Rankine cycle with R123 as the working fluid.

The engine of a vehicle does not work in a steady state when it is driven. Determining how to recover the exhaust gas waste heat of a vehicle engine using an ORC system is still a tough task for the automotive industry because there are several obstacles that must be overcome. First, a proper expander needs to be developed that can adapt to the various working conditions of a vehicle engine with a high efficiency. Second, a compact evaporator that can withstand the high temperatures of engine exhaust gas for a long duration must be created. Third, developing of an appropriate working fluid that can accommodate well to the hardware and provide the highest output power is also a hard task to realize. Last, keeping the entire ORC system safety and offering a durable life when operating within the vehicle engine environment, is also a significant challenge. Diego et al. [18] studied three configurations of Rankine cycles for waste heat recovery in a hybrid vehicle. A supercritical, reciprocating Rankine engine for waste heat recovery of diesel engines was proposed by Teng et al. [19,20]. Water and ethanol as working fluids were considered for two kinds of ORC for waste heat recovery of gasoline engines by Ringler et al. [21]. Atan [22] studied heat recovery equipment (i.e., a generator) for an absorption air-conditioning system when the working fluid was a combination of water and lithium bromide.

If the ORC system structure and the working conditions are setup properly, the selection of the working fluid has a significant impact on system performance. Because the engine exhaust gas states vary widely when a vehicle is running, it is important to define the operating conditions of ORC that achieve the maximum utilization of the waste heat. In this paper the operating conditions of an ORC system using a single screw expander for recovering the vehicle engine waste heat were analyzed. The thermodynamic models of nine various organic working fluids under these constrained situations were fabricated and calculated using a Matlab application with REFPROP. The performances of each fluid were compared in a feasible pre-defined region based on the evaporating pressure and condensing temperature. To accommodate the transient, operational characteristics of a vehicle engine, the control strategy of an ORC system is discussed based on the calculation results.

2. Thermodynamic modeling of ORC

The schematic of a simple organic Rankine cycle is depicted in Fig. 1. In this paper, this ORC structure is named A type, where the working fluid is pumped from the reservoir to the high pressure pipe line. The waste heat is absorbed in the evaporator under constant pressure and then shifts into a saturated gas state. The high enthalpy saturated gas is then expanded in the single screw expander. At the same time, power is generated and output to the generator. A prototype of the expander assembly examined is shown in Fig. 2. (The single screw expander was invented by Beijing University of Technology, China. Its rated power is 10 kW [23].)

Various working fluids usually can be classified into three categories according to the slope of the saturation vapor line in a T–s diagram. A dry fluid has a positive slope; a wet fluid has a negative slope, whereas an isentropic fluid has infinitely large slopes. All the working fluids investigated in this study are dry or

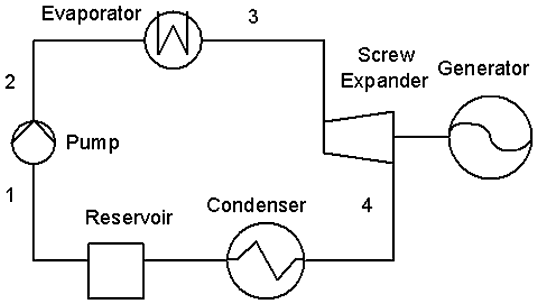

Fig. 1. Schematic of A type of ORC.

isentropic fluids, which translate into superheated gas states after expansion. Subsequently, the low pressure superheated gas is cooled down to saturated liquid in the condenser.

The thermal efficiency of an ORC system can be augmented by adding an internal heat exchanger (IHE). The schematic of an ORC with an IHE is delineated in Fig. 3 and is denoted as B type. The high temperature working fluid exhausted from the screw expander is transported to the inlet of low pressure side of IHE. The low-temperature working fluid exported from the pump is conveyed to the inlet of high pressure side of IHE. The heat is transferred from the low pressure side to high pressure side in IHE.

The T–s diagrams of these two ORCs are shown in Fig. 4. The pressure and heat loss of the working fluid in the pipes were neglected. At state point 1, the working fluid condition is at a saturated liquid state. At state point 3 it locates at the saturated vapor line. The pump process is from 1 to 2, where 1–2s is the corresponding isentropic compression process. The state point at the high pressure side outlet of the IHE is 2a. The evaporation process is represented as 2–3 for the A type of ORC, and 2a–3 for the B type, respectively. The expansion process in the single screw expander is 3–4. If the IHE is added, process 4–4a describes what occurs in the low pressure side. Process 3–4s is the relevant isentropic expansion process.

The mathematical model of the A type of ORC is expressed by equations (1)–(13). The work consumed by the pump $\dot{W}_p$ is listed in equation (1):

$$\dot{W}_p = \dot{m}(h_2 - h_1) = \frac{\dot{m}(h_{2s} - h_1)}{\eta_p} \quad (1)$$

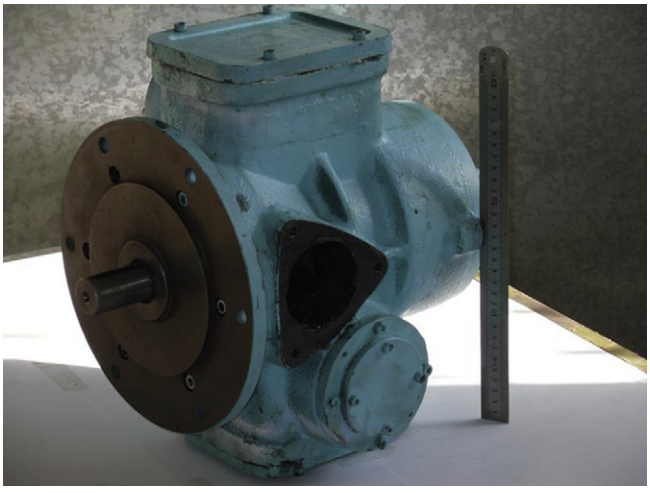

Fig. 2. Prototype of the single screw expander.

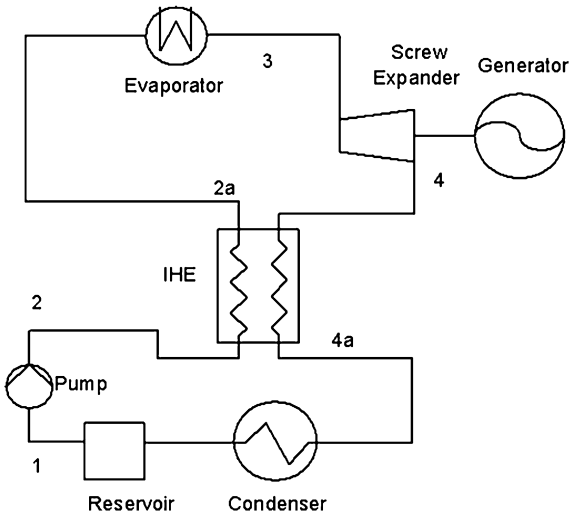

Fig. 3. Schematic of B type of ORC.

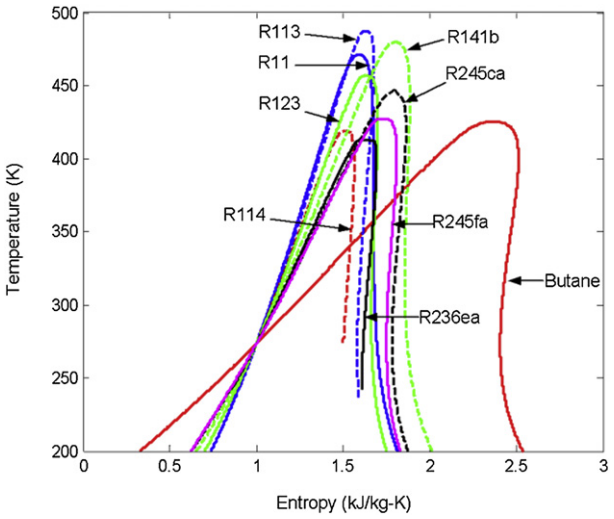

Fig. 5. Schematic of *T–s* plots of the selected work fluids.

The heat addition from the waste gas to the working fluid $\dot{Q}_e$ is denoted as

$$\dot{Q}_e = \dot{m}(h_3 - h_2) \tag{2}$$

The work generated by the single screw expander $\dot{W}_s$ is calculated by equation (3):

$$\dot{W}_s = \dot{m}(h_3 - h_4) = \dot{m}(h_3 - h_{4s})\eta_s \tag{3}$$

The heat rejection from the condenser $\dot{Q}_c$ is characterized by

$$\dot{Q}_c = \dot{m}(h_4 - h_1) \tag{4}$$

Exergy is the maximum amount of work that can be done by a subsystem as it approaches thermodynamic equilibrium with its surroundings by a sequence of reversible processes [24]. The exergy of a subsystem is a measure of its "distance" from equilibrium. Thus it can signify the quality of the energy of the subsystem. Exergy destruction rate labels the loss of exergy during the process. It can be obtained from the exergy balance equations using an exergy analysis method [25–27]. The exergy destruction rates of the pump process $\dot{I}_p$, the evaporation process $\dot{I}_e$, the expansion process $\dot{I}_s$ and the condensation process $\dot{I}_c$ are delineated by equations (5)–(8), respectively:

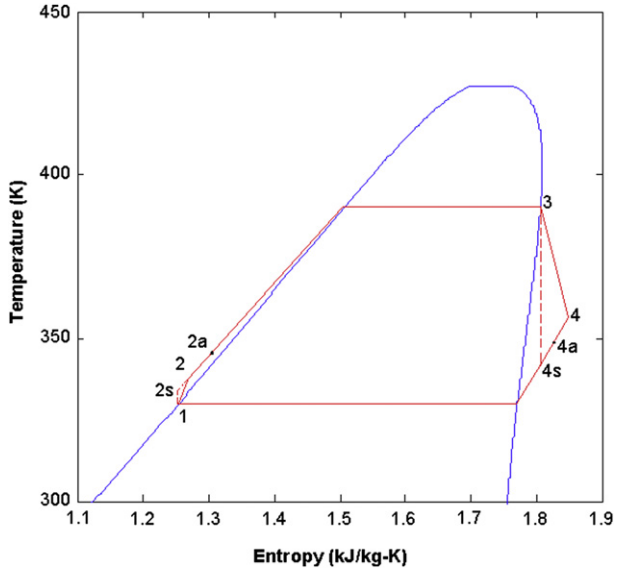

Fig. 4. *T–s* diagram of ORCs.

$$\dot{I}_p = T_0\dot{m}(s_2 - s_1) \tag{5}$$

$$\dot{I}_e = T_0\dot{m}\left[(s_3 - s_2) - \frac{h_3 - h_2}{T_H}\right] \tag{6}$$

$$\dot{I}_s = T_0\dot{m}(s_4 - s_3) \tag{7}$$

$$\dot{I}_c = T_0\dot{m}\left[(s_1 - s_4) - \frac{h_1 - h_4}{T_L}\right] \tag{8}$$

The net power output $\dot{W}_n$ is denoted by

$$\dot{W}_n = \dot{W}_s - \dot{W}_p \tag{9}$$

The ORC system thermal efficiency η_{th} is computed as:

$$\eta_{th} = \frac{\dot{W}_s - \dot{W}_p}{\dot{Q}_e} \tag{10}$$

Equation (11) calculates the total exergy destruction rate $\dot{I}_{tot}$:

$$\dot{I}_{tot} = \dot{I}_p + \dot{I}_e + \dot{I}_s + \dot{I}_c = T_0\dot{m}\left[-\frac{h_3 - h_2}{T_H} - \frac{h_1 - h_4}{T_L}\right] \tag{11}$$

The expanding pressure ratio π is computed by

$$\pi = \frac{P_3}{P_4} \tag{12}$$

The volumetric flow rate at the inlet of the screw expander $\dot{V}_3$ is calculated according to

$$\dot{V}_3 = \frac{\dot{m}}{\rho_3} \tag{13}$$

If the IHE is taken into account for the B type of ORC model, the model of the A type needs to be revised according to equations (14)–(20). The pressure loss and heat rejection to the environment of the IHE were not considered. The effectiveness of IHE can be expressed as [28]:

$$\varepsilon = \frac{T_4 - T_{4a}}{T_4 - T_2} \tag{14}$$

Table 1
The properties of the selected pure work fluids.

Substance		Molecular mass [kg/kmol]	T_b[a] [K]	P_{cr}[b] [MPa]	T_{cr}[c] [K]	ASHRAE 34 safety group	Atmospheric life time [yr]	ODP[d]	GWP[e] [100 yr]
1	R245fa	134.05	288.05	3.64	427.2	B1	7.2	0	950
2	R245ca	134.05	298.28	3.925	447.57	n.a.	6.6	0	610
3	R236ea	152.04	279.34	3.502	412.44	n.a.	8	0	1200
4	R141b	116.95	305.2	4.46	479.96	n.a.	9.3	0.086	700
5	R123	152.93	300.97	3.662	456.83	B1	1.3	0.012	120
6	R114	170.92	276.74	3.257	418.83	A1	300	0.85	9800
7	R113	187.38	320.74	3.392	487.21	A1	85	0.9	6130
8	R11	137.37	296.86	4.408	471.11	A1	45	1	4600
9	Butane	58.122	272.6	3.796	425.12	n.a.	9.3	0.12	725

n.a.: non-available.
[a] T_b: normal boiling point.
[b] P_{cr}: critical pressure.
[c] T_{cr}: critical temperature.
[d] ODP: ozone depletion potential, relative to R11.
[e] GWP: global warming potential, relative to CO_2.

The exergy destruction of the IHE is modeled as

$$\dot{I}_{IHE} = T_0\dot{m}[(s_{4a} - s_4) + (s_{2a} - s_2)] \quad (15)$$

The corresponding evaporation process equations (2) and (6) are replaced by equations (16) and (17):

$$\dot{Q}_e = \dot{m}(h_3 - h_{2a}) \quad (16)$$

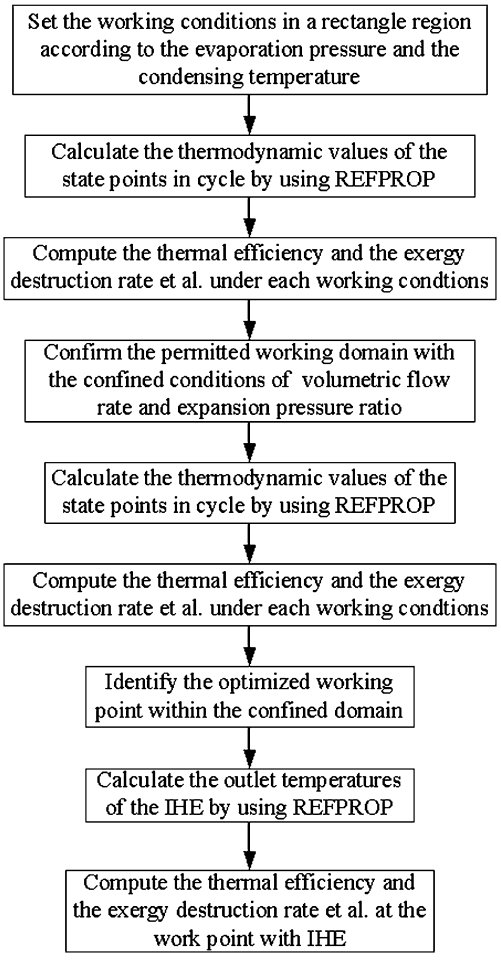

Fig. 6. Work flow diagram for the ORC performance calculation.

$$\dot{I}_e = T_0\dot{m}\left[(s_3 - s_{2a}) - \frac{h_3 - h_{2a}}{T_H}\right] \quad (17)$$

The condensation process is modeled as equations (18) and (19) instead of (4) and (8):

$$\dot{Q}_c = \dot{m}(h_{4a} - h_1) \quad (18)$$

$$\dot{I}_c = T_0\dot{m}\left[(s_1 - s_{4a}) - \frac{h_1 - h_{4a}}{T_L}\right] \quad (19)$$

The total exergy loss is calculated as

$$\dot{I}_{tot} = T_0\dot{m}\left[-\frac{h_3 - h_{2a}}{T_H} - \frac{h_1 - h_{4a}}{T_L}\right] \quad (20)$$

3. Simulation and performance analysis

Fluid selection is one of the most important contributors to overall cycle performance. Fluid thermodynamics, material compatibility, flammability, toxicity and other properties must be considered with respect to the vehicle's needs. Desirable characteristics of the working fluids include appropriate boiling point temperature, low latent heat, high critical temperature and pressure, suitable specific volume, low density and surface tension, high thermal conductivity, high thermal stability, non-corrosive, non-toxic, and compatibility with engine

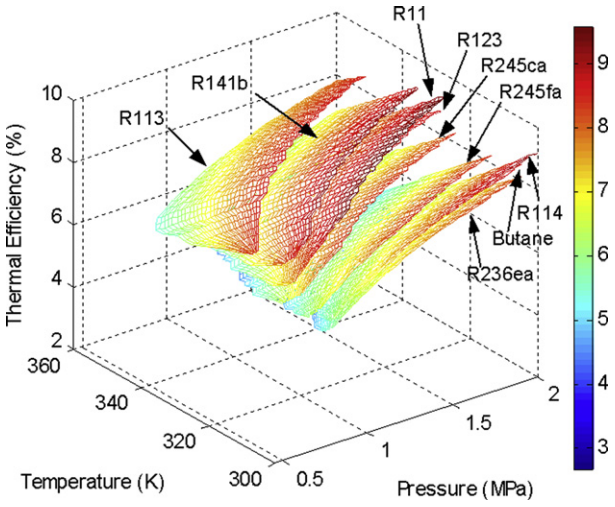

Fig. 7. System thermal efficiency comparison of different working fluids for A type.

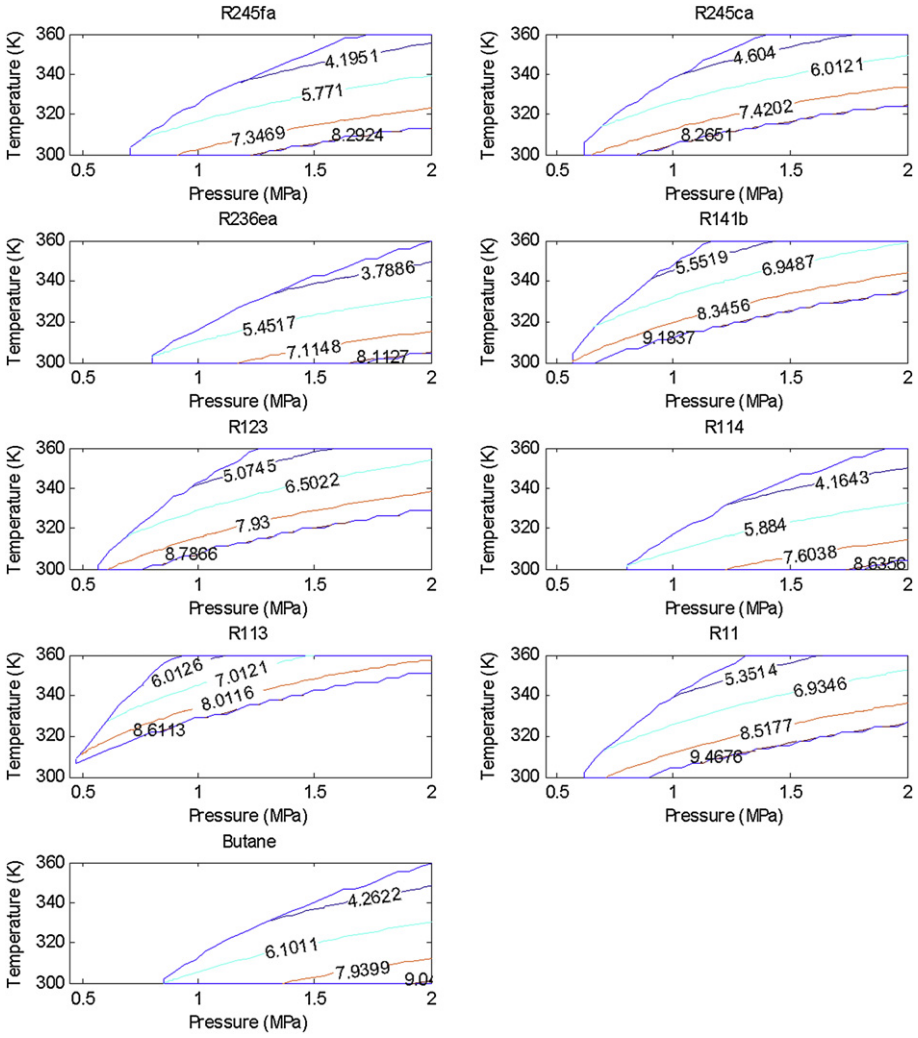

Fig. 8. Contour maps of the thermal efficiency for A type.

materials. Nine pure organic working fluids were selected; the *T*–*s* diagrams are plotted together in Fig. 5. Wet working fluids such as water were not included because of their large latent heat vaporization properties, which are not appropriate for waste heat-recovery applications. The physical and chemical properties of the selected working fluids and their impacts on the environment are listed in Table 1.

Considering the operational status of an ORC system assembled on the vehicle and the design parameters of the single screw expander, the constraining conditions of the model are listed as follows:

(1) The working fluids were selected as pure fluids whose boiling points are greater than 270 K.
(2) The heat quantity provided by the exhaust gas was sufficient to meet the ORC operation.
(3) The condensing temperature ranged from 300 K to 360 K.
(4) The evaporating pressure ranged from 0.2 MPa to 2 MPa.
(5) The reference temperature was set to 273 K.
(6) The high temperature heat source of ORC was set to 600 K and the low-temperature heat source was set to 300 K.
(7) The net power out from the ORC was set to 10 kW. (The value of 10 kW is specified for experimental study. In fact, the rated power of ORC should be decided according to the practical configurations of vehicle engine. A relevant analysis can be referenced in [29].)
(8) The pressure ration of the screw expander was limited to 8.
(9) The maximum volumetric flow of the working fluid at the outlet of the expander was 20 L/s.
(10) The efficiency of the pump was set to 0.8.

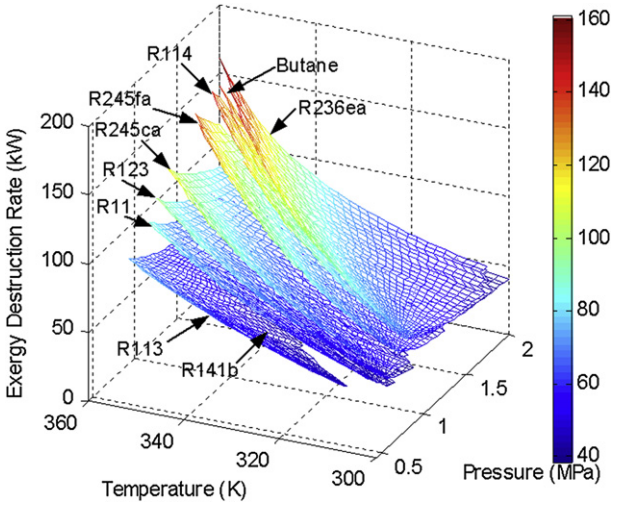

Fig. 9. System exergy destruction rate comparison for A type.

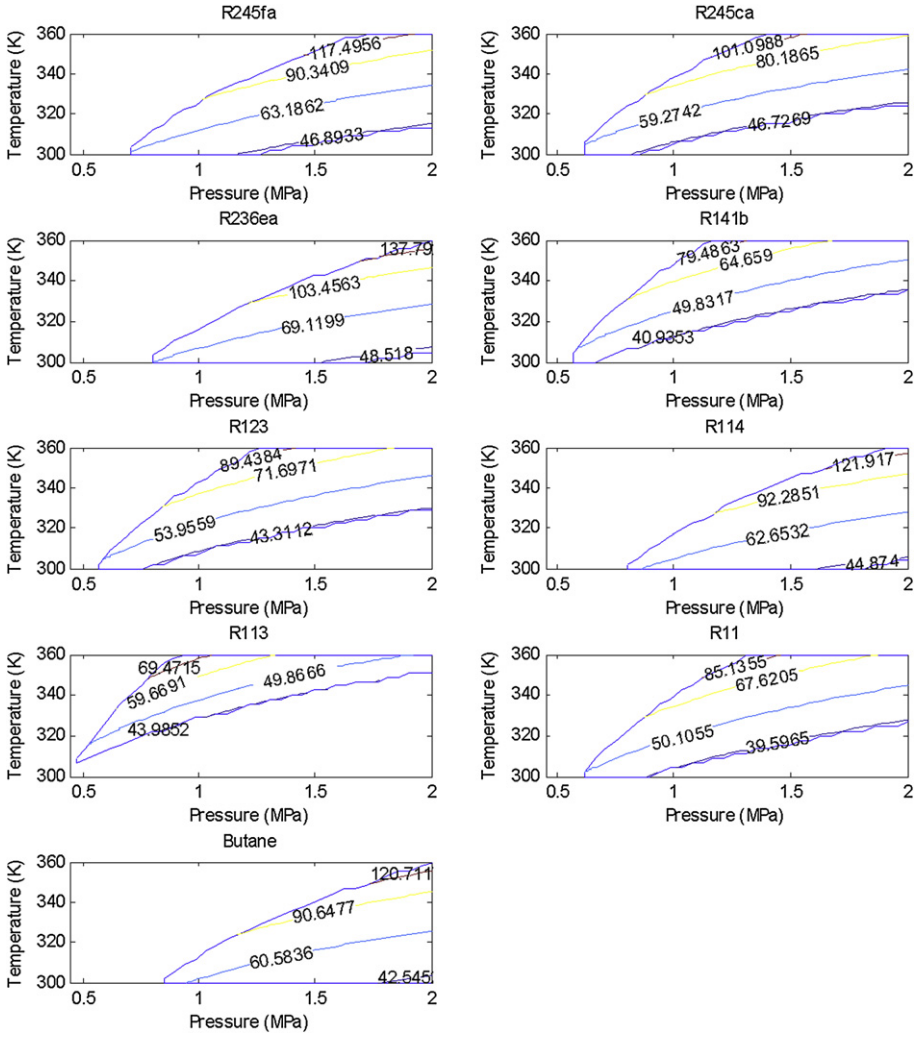

Fig. 10. Contour maps of the exergy destruction rate for A type.

(11) The efficiency of the screw expander was set to 0.55.

In addition, to calculate the B type ORC performance, the following constraint condition was added:

(12) The effectiveness of IHE was assumed to be 0.90.

The working fluid, with its boiling point lower than 270 K, reaches a superheated gas state in the ambient environment. This is not beneficial for the storage on the vehicle. Normally, the exhaust gas temperature of a vehicle engine varies from 400 K to 1100 K [29,30]. The pertinent evaporating temperature of the working fluid could be set from 370 K or lower to 1000 K or higher. Generally, the maximum working pressure an evaporator could tolerate ranges from 0.2 MPa to 2 MPa. This scope is smaller than the evaporating temperature domain noted above, so it is appropriate to choose evaporating pressure as the comparison parameter. The working pressure of the condenser is not very high and could be considered for a large region, but condensing temperature is constrained by the working conditions of the internal combustion engines on the vehicles. Thus condensing temperature is used as the independent variable instead of condensing pressure. Conditions (5) and (6) are used for the exergy analysis. Conditions (7)–(11) are defined by the design parameters of the single screw expander [31].

The model was developed in Matlab [32]. The thermodynamic parameters of the working fluids were calculated by REFPROP through a COM interface function. REFPROP was developed by the National Institute of Standards and Technology of the United States [33]. The uncertainties in REFPROP vary depending on the fluid, property, and thermodynamic state. The maximal uncertainties of

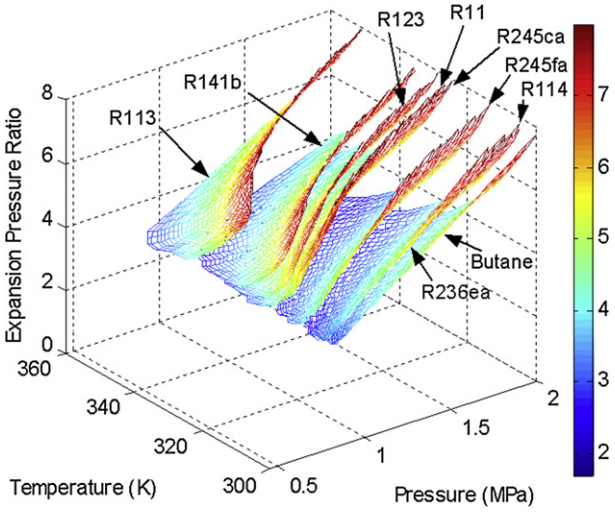

Fig. 11. Expansion pressure ratio comparison.

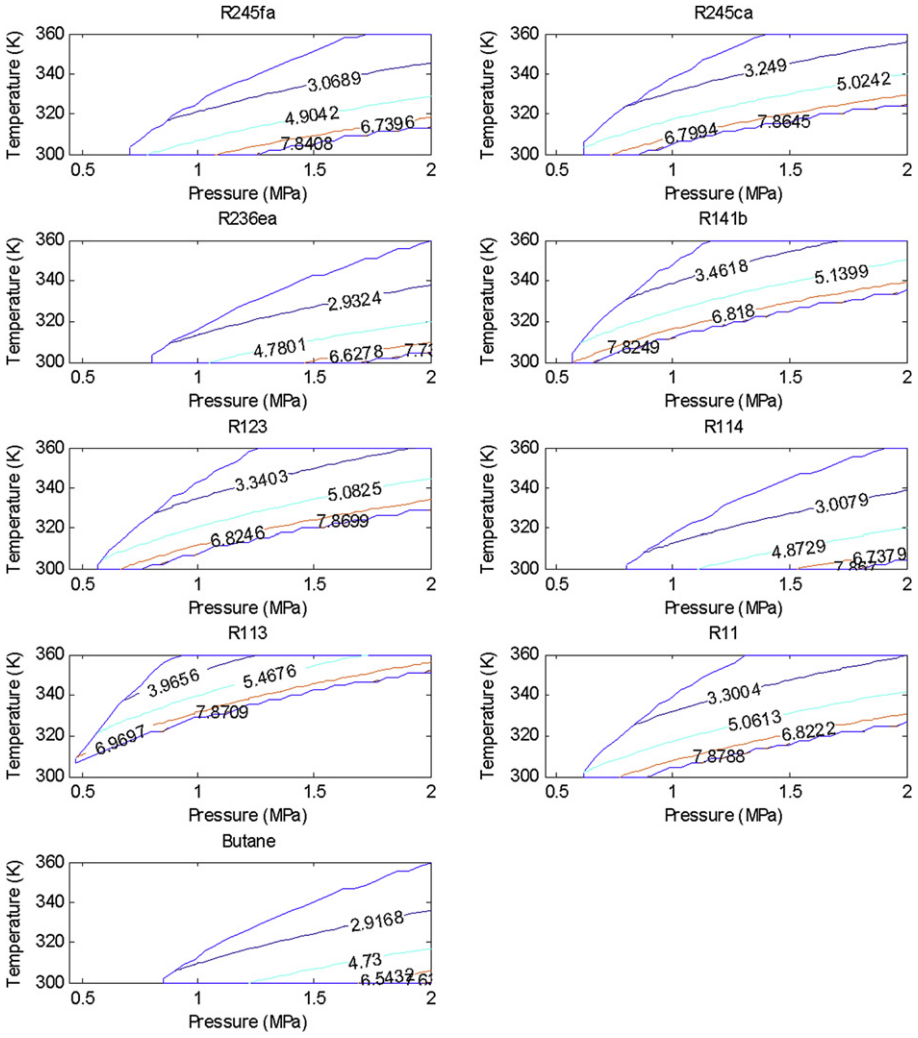

Fig. 12. Contour maps of the expansion pressure ratio.

the equation of state are no more than 0.2% in density for the liquid, and 0.4% for the vapor, and 0.4% in vapor pressure among all the selected organic working fluids. A detailed description of accuracy can be found from the NIST website for different working fluids.

The work flow diagram of the calculation algorithm in Matlab is shown in Fig. 6. Initially, the working points defined by the condensing temperature and the evaporating pressure were computed. The condensing temperatures selected were equidistant from 300 K to 360 K; the evaporating pressures were also equally distributed from 0.2 MPa to 2 MPa. Next, the thermodynamic values, such as entropy and enthalpy, for each A type state points were calculated for each working fluid. (Here, REFPROP was treated as a COM function in Matlab.) Then the ORC performances based on these state points were calculated according to equations (1)–(13). Subsequently, the constrained conditions of (4) and (5) were taken into account, when the ORC working region defined by the evaporating pressure and the condensing temperature was trimmed from a rectangle into an irregular shape. This irregular shape represents the feasible working region. The working points were redesignated within the feasible region, and the ORC performances were computed again based on the new working point definitions.

Comparing the ORC performances of A type for different working fluids, the results were plotted as various surfaces and contour maps and are shown in Figs. 7–17. ORC thermal efficiency is the most important index used to estimate performance. System thermal efficiency of ORC varies with the condensing temperature and the evaporating pressure in the feasible region, and formed a surface as shown in Fig. 7. The results indicate that thermal efficiency increases as condensing temperature diminishes, and decreases as

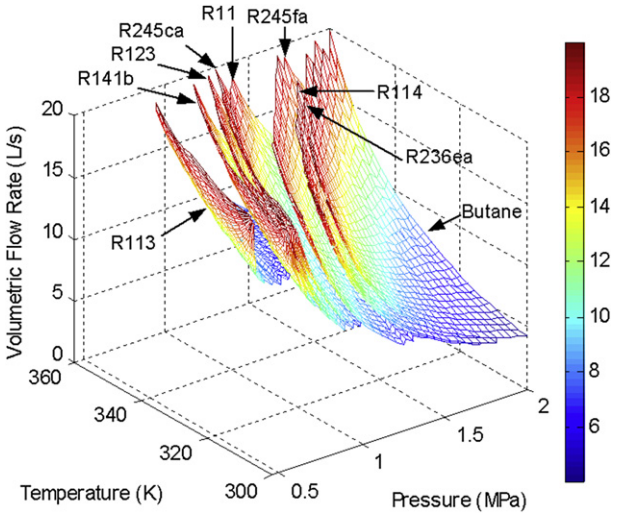

Fig. 13. Volumetric flow rate comparison.

evaporating pressure recedes. The impact of condensing temperature is larger than that of evaporating pressure. When the operating conditions of different working fluids are identical, the sequence of system thermal efficiency from maximum to minimum is R113, R141b, R11, R123, R245ca, R245fa, R114, Butane, R236ea. The reasons can be explained based on a simplied ORC model [8,20]. Theoretically, the thermal efficiency of A type of ORC can be expressed as

$$\eta_{th} = 1 - \left[\left(\frac{1 - T_e/T_{cr}}{1 - T_c/T_{cr}}\right)^n + \left(\frac{1 - T_m/T_{cr}}{1 - T_c/T_{cr}}\right)^n \left(\frac{nT_m/T_{cr}}{1 - T_m/T_{cr}} + 1\right) \frac{T_e/T_{cr} - T_c/T_{cr}}{T_m/T_{cr}}\right]^{-1} \quad (21)$$

where T_m and n can be denoted as follows:

$$T_m = \frac{T_e + T_c}{2} \quad (22)$$

$$n = \left(0.00264 \times \frac{L_b}{RT_b} + 0.8794\right)^{10} \quad (23)$$

For most working fluids, the exponent n in equation (21) varies in a narrow range between 0.375 and 0.380 [34,35]. Using R245fa as an example, its value equals to 0.381. Considering the working point of $T_e = 390$ K and $T_c = 340$ K, the thermal efficiency of R245fa calculated according to equation (21) is 10.12%. When the evaporating temperature is reduced by 1 K, the thermal efficiency decreases by 0.1%; but when the condensing temperature is decreased by 1 K, the thermal efficiency rises by 0.27%. The deviation of the thermal efficiency values with regard to the condensing temperature is two times greater than that with respect to the evaporating temperature. Therefore, the influence of condensing temperature on system thermal efficiency is greater than of evaporating pressure.

Considering the selected working fluids, when T_e and T_c are fixed to a pair of identical values, their thermal efficiencies are merely dependent on their critical temperatures T_{cr} and n values. These two properties are determined by the working fluids' molecular compositions and structures. Essentially, it is the discrepancy of the molecular forces generated by different working fluids that causes the variation of these thermodynamic properties.

In searching for the working condition in which the greatest thermal efficiency is achieved, the contour maps for each organic working fluid are plotted in Fig. 8 for comparison. The feasible region is limited by two boundary lines. The upper one is constrained by the maximum volumetric flow rate; the lower one is limited by the maximum pressure ratio. Four contour lines are added in each map, and the gradient for these lines is explained below, where the maximum and minimum thermal efficiencies in the feasible region can be found, respectively. The difference of these two values $\Delta\eta$ is defined as

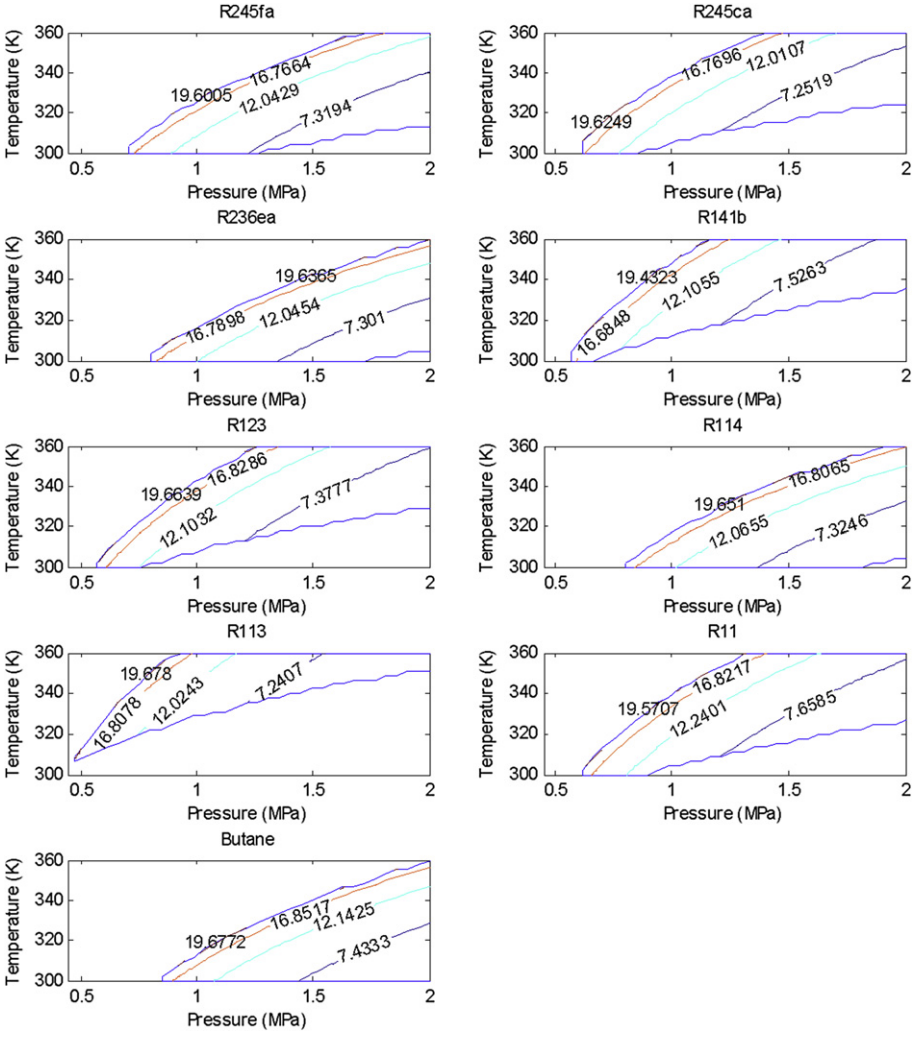

Fig. 14. Contour maps of the volumetric flow rate.

$$\Delta\eta = \eta_{max} - \eta_{min} \quad (24)$$

The thermal efficiencies of the contour lines are configured according to the following vector:

$$[\eta_{max} - 0.02\Delta\eta \ \eta_{max} - 0.2\Delta\eta \ \eta_{max} - 0.5\Delta\eta \ \eta_{max} - 0.8\Delta\eta] \quad (25)$$

This approach is also applied in all the following contour maps. The operating region, where the degradation of the thermal efficiency is within 20% of the maximum value η_{max}, is defined as the optimal working region. The relative optimal working regions of various working fluids are shown as the "belt" shape in Fig. 8.

When the ORC system is assembled on the vehicle, the operational conditions during the transient process should be controlled within the optimal working region to maintain a high thermal efficiency. Because the ambient temperature varies with the seasons during the year, the condensing temperature of the ORC can be controlled by a fan to regulate it as close as possible to the current ambient temperature. Accordingly, the evaporating pressure should be adjusted to operate inside the optimal working region. When the vehicle is running in a transient process, the waste heat generated by the engine also varies. This causes evaporating pressure variation in the evaporator. When this occurs, the mass flow rate of the working fluid needs to be controlled to keep the evaporating pressure in the optimal region with regard to the relevant condensing temperature. An optimal working region that can cover a wide range of condensing temperatures as well as evaporating pressures is advantageous. From the results in Fig. 8, the optimal working regions of R245fa, R245ca, R141b, R11, R123, and R113 are shown to satisfy this requirement.

The ORC system exergy destruction rate comparison is delineated in Fig. 9. The corresponding contour maps are shown in Fig. 10. On the same surface, the exergy destruction rate is relatively small when the ORC is working in the high thermal efficiency region. But it increases drastically as the ORC moves to its low thermal efficiency region. The working fluid with a higher thermal efficiency manifests lower exergy loss. The reason is, for a specific 10 kW net power output, the heat addition will increase rapidly if thermal efficiency becomes smaller.

Comparisons of expanding pressure ratios are shown in Figs. 11 and 12. Those working points with a higher pressure ratio result in larger thermal efficiency in the feasible working region. The maximum pressure ratio is limited to eight based on the constraints of the design of the single screw expander, such as leakage. Thus the maximum thermal efficiency could not be improved further.

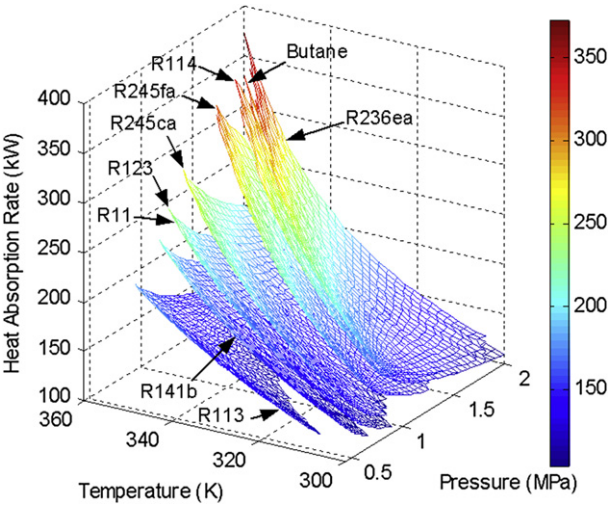

Fig. 16. Heat absorption rate comparison for A type.

When the pressure ratio rises in the feasible region, the deviation between the evaporating temperature and condensing temperature increases. This causes an incremental change to the thermal efficiency, which can be evaluated using equation (21).

When the condensing temperatures of the selected working fluids are given a specific constant value, the corresponding vapor pressures can be calculated based on the Riedel method [34]:

$$\ln P_{vpr} = A - B/T_r + C \ln T_r + DT_r^6 \quad (26)$$

where the reduced vapor pressure P_{vpr} and the reduce temperature T_r are defined as

$$P_{vpr} = P_{vp}/P_{cr} \quad (27)$$

$$T_r = T/T_{cr} \quad (28)$$

Because various working fluids have distinct coefficient values, the corresponding condensing pressures are also different. When the pressure ratios are set to the maximum value, the pertinent maximal evaporating pressures are also distinct. This is why the lower boundary lines of the feasible working regions deviate among the selected working fluids.

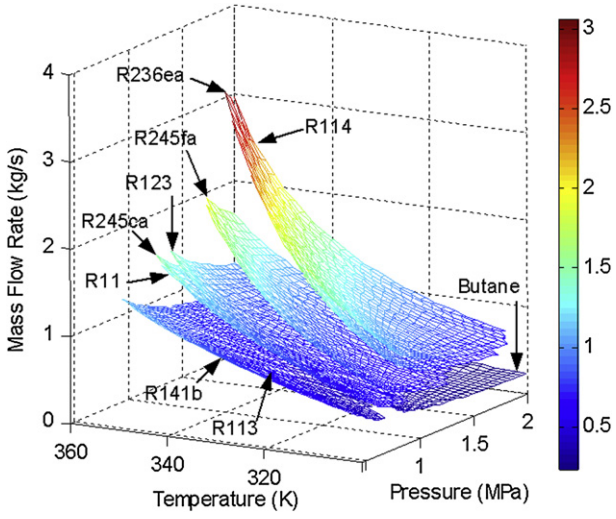

Fig. 15. Mass flow rate comparison.

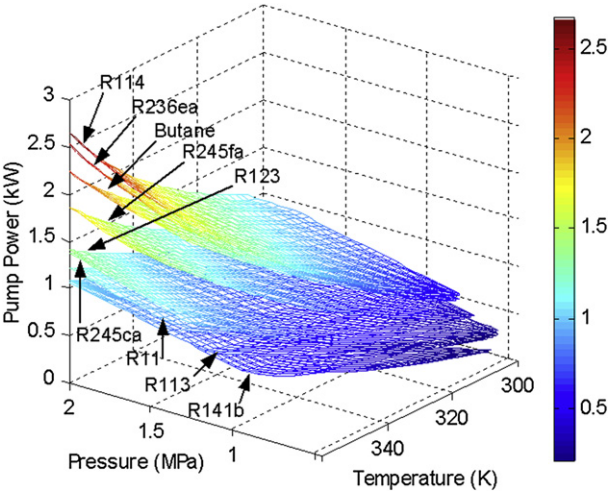

Fig. 17. Pump power comparison.

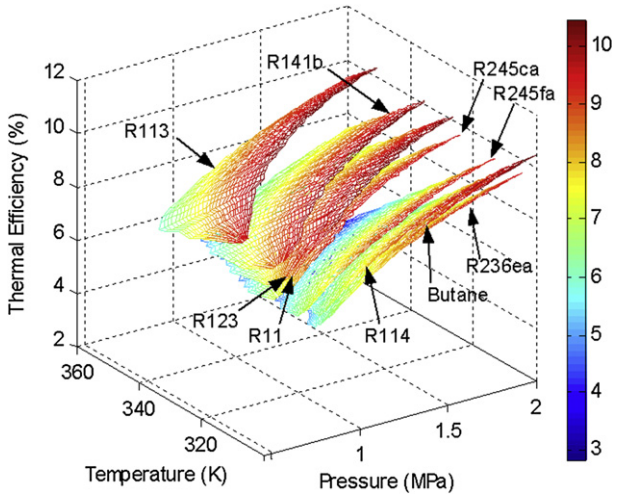

Fig. 18. System thermal efficiency comparison for B type.

The consequences of the volumetric flow rates are plotted in Figs. 13 and 14. It shows that the practical values reach their maximum values in the low thermal efficiency region. As mentioned previously, the mass flow rate increases when thermal efficiency decreases. When the evaporating pressure is configured to a constant value, the value of the specific volume of the working fluid remains stable, and which can be calculated according to the pertinent equation of states [36]. As a result, the volumetric flow rate will be enhanced synchronously with the mass flow rate. In fact, the volumetric flow rate in the inlet of the developed single screw expander cannot exceed 20 L/s, therefore, the discrepancies of the upper boundary lines are generated.

The mass flow rates are displayed in Fig. 15. The heat absorption rate from the exhausted gases is exhibited in Fig. 16. The pump power is depicted in Fig. 17. As formerly mentioned, when the thermal efficiency decreases in the feasible region, the mass flow rate as well as the heat addition increases. The pump power will also improve incrementally with the mass flow rate.

The performances of B type for the selected working fluids were calculated according to equations (14)–(20). The thermal efficiencies dependent on the condensing temperature and the evaporating pressure are shown in Fig. 18. The contour maps of the thermal efficiency surfaces are plotted in Fig. 19. The results show that at a fixed working point the order of the thermal efficiency value from maximum to minimum is R113, R141b, R123, R11, R245ca, R245fa, R114, Butane, R236ea. The sequence of R11 and R123 is reversed comparing with the A type. Apparently, the boundaries of the feasible working regions are the same as A type, but the performances of B type are better than the corresponding

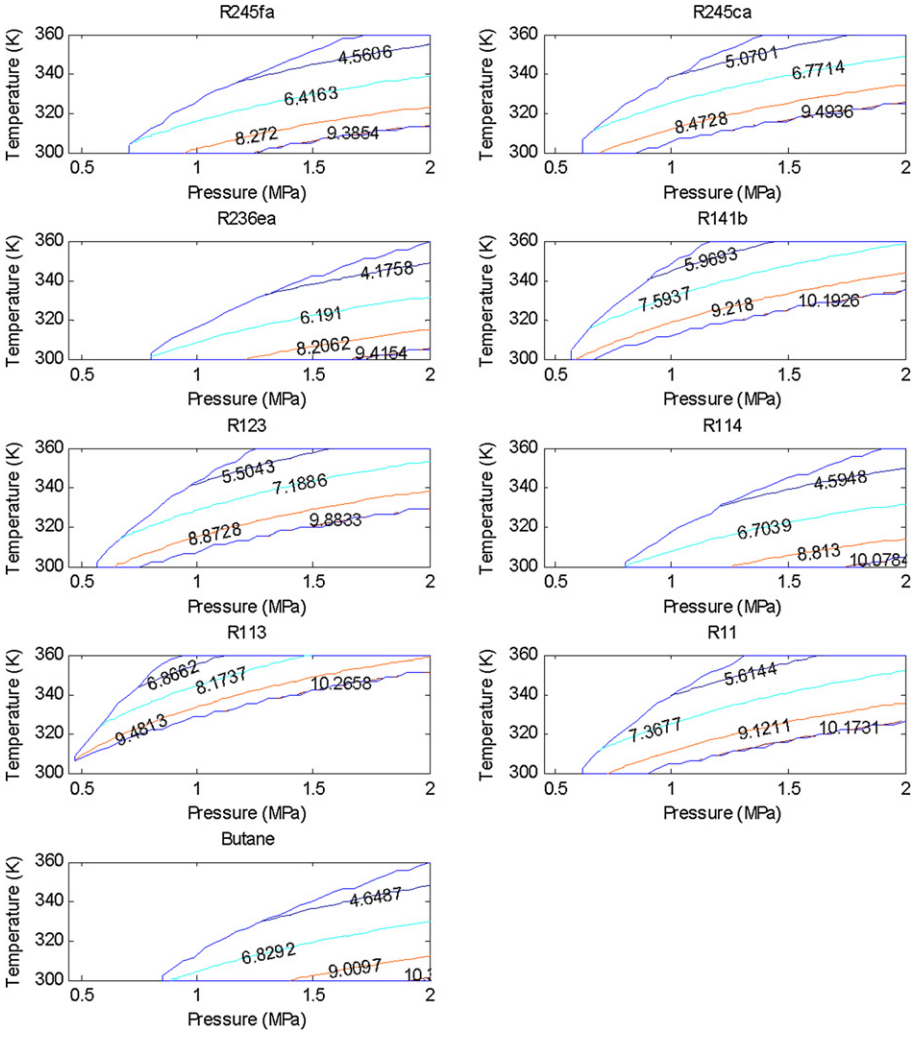

Fig. 19. Contour maps of the thermal efficiency for B type.

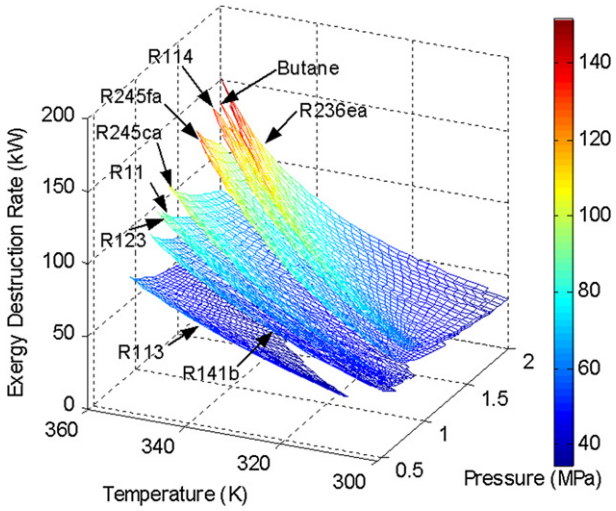

Fig. 20. System exergy destruction rate comparison for B type.

ones of A type. The working fluid in the IHE, before entering the expander, absorbs the heat from the working fluid exhausted from the single screw expander – the enthalpy of the working fluid is enhanced before entering the evaporator. Comparing the condition of the same net power output, the heat addition of B type is less than of A type. Therefore, its thermal efficiency is improved. The addition of IHE cannot modify constrained conditions (4) and (5), which are limited by the single screw expander, thus, the boundary lines are not revised.

The outcomes of the exergy destruction rates for B type are displayed in Figs. 20 and 21. All exergy destruction rates of B type are reduced compared with the relative results of A type. The range extends from the maximum value of 19.31% for R113 to the minimum value of 8.38% for R11. The evaporation process from state point 2 or 2a to state point 3 needs a large amount of heat and will generate plenty of exergy destruction. To diminish this exergy destruction rate, a working fluid with low latent heat and high thermal conductivity is preferred. Working fluids with lower latent heat value will be easier to gasify, thus, more saturated vapors will be generated under an identical heat addition quantity condition during the evaporation process. Because this will enlarge the output power of the expander, thermal efficiency is enhanced. The working fluid with a high thermal conductivity coefficient will facilitate the design of the evaporator and reduce the size, allowing it to be deployable on a vehicle. Therefore, the working fluid with low latent heat and high thermal conductivity is more suitable for a vehicle engine waste heat-recovery application.

Maximum thermal efficiency is achieved at the edge of the optimal working region. The best working points for each working

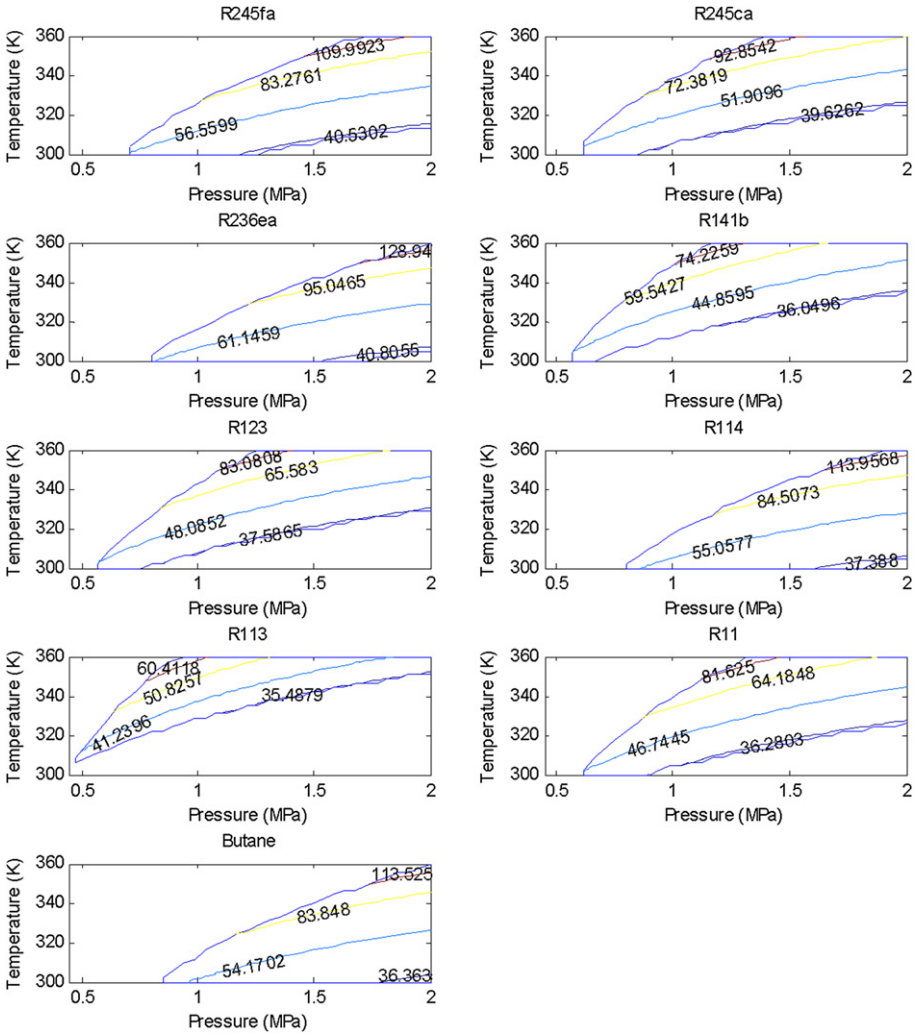

Fig. 21. Contour maps of the exergy destruction rate for B type.

Table 2
Comparison of the optimal working conditions of different working fluids for 10 kW net power output.

	Substance	η_{th} [%]	P_e [MPa]	T_e [K]	$\dot{Q}_e$ [kW]	T_c [K]	P_c [MPa]	π	$\dot{m}$ [kg/s]	$\dot{V}_3$ [L/s]	$\dot{W}_p$ [kW]	$\dot{W}_s$ [kW]	$\dot{I}_{tot}$ [kW]	$\dot{I}_p$ [kW]	$\dot{I}_e$ [kW]	$\dot{I}_s$ [kW]	$\dot{I}_c$ [kW]
(a) Selected working condition for A type of ORC																	
1	R245fa	8.40	1.4923	380.90	119.08	304.44	0.1874	7.964	0.4988	5.738	0.615	10.615	45.080	0.1101	35.582	7.214	2.174
2	R245ca	8.63	1.4923	395.05	119.64	315.56	0.1882	7.929	0.4815	5.666	0.584	10.584	45.336	0.1009	32.607	6.897	5.731
3	R236ea	8.22	1.7231	377.51	121.60	300.00	0.2196	7.848	0.5979	4.882	0.791	10.791	46.229	0.1436	37.766	7.375	0.945
4	R141b	9.28	1.7231	420.42	107.80	328.89	0.2173	7.929	0.4054	5.137	0.650	10.650	39.947	0.1077	24.746	6.773	8.321
5	R123	8.88	1.5385	406.00	112.59	320.00	0.1926	7.986	0.5458	5.614	0.652	10.652	42.128	0.1110	28.649	6.913	6.455
6	R114	8.75	1.8154	385.81	114.28	300.00	0.2275	7.981	0.6722	4.550	0.919	10.919	42.899	0.1668	34.318	7.416	0.998
7	R113	8.68	1.1231	418.61	115.23	331.11	0.1411	7.959	0.6026	7.673	0.499	10.499	43.331	0.0821	26.791	6.371	10.087
8	R11	9.57	1.400	399.72	104.46	313.33	0.1754	7.981	0.4919	6.557	0.523	10.523	38.427	0.0909	27.178	7.207	3.951
9	Butane	9.17	2.000	387.51	109.10	300.00	0.2580	7.752	0.2330	4.294	0.887	10.887	40.541	0.1610	32.127	7.475	0.778

	Substance	η_{th} [%]	P_e [%]	T_e [K]	$\dot{Q}_e$ [kW]	T_c [K]	P_c [MPa]	T_4 [K]	T_2 [K]	T_{4a} [K]	T_{2a} [K]	π	$\dot{m}$ [kg/s]	$\dot{V}_3$ [L/s]	$\dot{W}_p$ [kW]	$\dot{W}_s$ [kW]	$\dot{I}_{tot}$ [kW]	$\dot{I}_p$ [kW]	$\dot{I}_e$ [kW]	$\dot{I}_s$ [kW]	$\dot{I}_c$ [kW]	$\dot{I}_{IHE}$ [kW]
(b) Selected working condition for B type of ORC																						
1	R245fa	9.51	1.4923	380.90	105.16	304.44	0.1874	337.84	305.09	308.36	325.42	7.964	0.4988	5.738	0.615	10.615	38.746	0.1101	29.859	7.214	1.273	0.290
2	R245ca	9.61	1.4923	395.05	104.10	315.56	0.1882	351.62	316.18	319.72	339.27	7.929	0.4815	5.666	0.584	10.584	38.264	0.1009	26.729	6.897	4.234	0.303
3	R236ea	9.55	1.7231	377.51	104.71	300.00	0.2196	334.82	300.78	304.19	322.87	7.848	0.5979	4.882	0.791	10.791	38.545	0.1436	30.662	7.375	0.014	0.350
4	R141b	10.30	1.7231	420.42	97.079	328.89	0.2173	363.76	329.78	333.18	351.52	7.929	0.4054	5.137	0.650	10.650	35.071	0.1077	21.032	6.773	6.969	0.190
5	R123	10.00	1.5385	406.00	100.04	320.00	0.1926	354.84	320.79	324.20	342.49	7.986	0.5458	5.614	0.652	10.652	36.420	0.1110	24.028	6.913	5.131	0.234
6	R114	10.22	1.8154	385.81	97.856	300.00	0.2275	337.91	300.98	304.67	325.17	7.981	0.6722	4.550	0.919	10.919	35.425	0.1668	27.465	7.416	0.016	0.362
7	R113	10.35	1.7692	444.74	96.595	346.67	0.2223	395.46	347.65	352.43	380.02	7.960	0.6195	4.666	0.829	10.829	34.851	0.1303	17.431	6.269	10.625	0.395
8	R11	10.29	1.400	399.72	97.178	313.33	0.1754	340.23	314.08	316.69	330.44	7.981	0.4919	6.557	0.523	10.523	35.116	0.0909	24.324	7.207	3.380	0.115
9	Butane	10.46	2.000	387.51	95.571	300.00	0.2580	335.45	301.08	304.52	324.26	7.752	0.2330	4.294	0.887	10.887	34.385	0.1610	26.469	7.475	0.013	0.267

fluid were selected and are listed in Table 2, where (a) displays the calculation results of A type, and (b) shows the consequences of B type. The working fluid that shows the highest thermal efficiency and the lowest exergy loss is R11 for A type and butane for B type. For instance, when R245fa is employed, the thermal efficiency of ORC is enhanced about 13.2% if the IHE is added. The evaporating pressure of R245fa is 1.4923 MPa, which is helpful for the evaporator design. When a vehicle engine is running under a series of transient working processes, the evaporating pressure and the condensing temperature of ORC should be regulated to approach the optimal stable values listed in Table 2 to maximize thermal efficiency.

The discrepancies of the largest thermal efficiencies among the working fluids are not so remarkable. The maximum values in Table 2 range from 8.22% to 9.57% for A type and from 9.51% to 10.46% for B type. Not only the thermodynamic performances of different working fluids should be evaluated but also their safety levels and environmental impacts must be taken into account. Butane is flammable. R11, R113 and R114 have high ODP and GWP. R141b will be forbidden in 2010 and R123 will be prohibited in 2020. Thereafter, R245fa and R245ca are the most suitable pure organic working fluids for an engine waste heat-recovery application when the environmental effects are evaluated.

4. Conclusion

In this study, several candidates of organic working fluids for an engine waste heat-recovery application were evaluated. The thermal efficiencies and exergy destruction rates of these working fluids have been investigated in an appropriate region defined by the evaporating pressure and the condensing temperature. The following consequences are concluded:

1. For the designed single screw expander, when the evaporating pressure and the condensing temperature vary in a certain region, the operation of the ORC system is constrained by the parameters of the expander. The optimal working regions of R11, R141b, R123, R245fa and R245ca are advantageous for the operation of ORC system.
2. In the feasible working region, the performances of R11, R141b, R113 and R123 are slightly higher than others. The thermal efficiency increases as the condensing temperature diminishes, and decreases as the evaporating pressure recedes. The impact of the condensing temperature is larger than that of evaporating pressure. Because waste heat generated by the engine varies when a vehicle is running, to maximize the utilization of the engine waste heat, the condensing temperature should be regulated as close as possible to the ambient temperature. At the same time, the mass flow rate of the working fluid needs to be controlled to keep the evaporating pressure in the optimal region.
3. If safety levels and environmental impacts are considered, R245fa and R245ca are the most suitable working fluids for an engine waste heat-recovery application.

The research work in this paper is focused on comparing ORC performance in terms of working fluids. A cost analysis with respect to the air-conditioning and relevant engine components of a class-B car was referenced. According to the analysis, a coarse evaluation of system cost of B type of ORC is less than 100$/kW for large amount of mass production. The experiments will be performed on the engine test bench. A comparative analysis between the experimental results (both from other researchers and ourselves) and theoretical outcomes will be accomplished in the future. Meanwhile, Component weight evaluation as well as effects on engine fuel consumption for an automotive application will be investigated.

Acknowledgements

This work was sponsored by the National Basic Research (973) Program of China (Grant #2011CB707202, Grant #2011CB710704), the National High-Tech Research and Development Program of China (863 Program) (Grant No. 2009AA05Z206), and the Funding Project for Academic Human Resources Development in Institutions of Higher Learning Under the Jurisdiction of Beijing Municipality (Grant No. PHR201008019). The authors would like to thank Professor Chongfang Ma and Professor Yuting Wu for their great support during the analysis process.

Nomenclature

h	enthalpy (kJ/kg)
s	entropy (kJ/kg K)
$\dot{m}$	mass flow rate (kg/s)
$\dot{I}$	exergy destruction rate (kW)
$\dot{W}$	power (kW)
T	temperature (K)
P	pressure (MPa)
t	time (s)
$\dot{Q}$	heat absorption rate (kW)
$\dot{V}$	volumetric flow rate (L/s)
L	latent heat (kJ/kg)
n	exponent of working fluid
R	universal gas constant (kJ/(mol K))
A, B, C, D	constant coefficients of the vapor pressure correlating equation
ln	natural logarithm

Greek letters

π	pressure ratio
η	efficiency (%)
ρ	density (kg/m^3)
ε	heat exchanger effectiveness (%)

Subscript

0	reference state
1,2,2s,2a,3,4,4s,4a	state points in cycle
p	pump
e	evaporator
s	single screw expander
c	condenser
n	net
th	thermal
tot	total
H	heat source
L	cold source
b	boiling point
cr	critical
m	moderate
r	reduced
vp	vapor pressure
max	maximum
min	minimum

Acronyms

ORC	organic Rankine cycle
ODP	ozone depletion potential
GWP	global warming potential
COM	component object model
IHE	internal heat exchanger

References

[1] Yu C, Chau KT. Thermoelectric automotive waste heat energy recovery using maximum power point tracking. Energy Convers Manage 2009;50:1506–12.
[2] Hettiarachchi HDM, Golubovic M, Worek WM, Ikegami Y. Optimum design criteria for an organic Rankine cycle using low-temperature geothermal heat sources. Energy 2007;32:1698–706.
[3] Saleh B, Koglbauer G, Wedland M, Fischer J. Working fluids for low-temperature organic Rankine cycles. Energy 2007;32:1210–21.
[4] Yamamoto T, Furuhata T, Arai N, Mori K. Design and testing of the organic Rankine cycle. Energy 2001;26:239–51.
[5] Tchanche BF, Papadakis G, Lambrinos G, Frangoudakis A. Fluid selection for a low-temperature solar organic Rankine cycle. Appl Therm Eng 2009;29:2468–76.
[6] Hung TC, Shai TY, Wang SK. A review of organic Rankine cycles (ORCs) for the recovery of low-grade waste heat. Energy 1997;22:661–7.
[7] Maizza V, Maizza A. Unconventional working fluids in organic Rankine-cycles for waste energy recovery systems. Appl Therm Eng 2001;21:381–90.
[8] Liu BT, Chien KH, Wang CC. Effect of working fluids on organic Rankine cycle for waste heat recovery. Energy 2004;29:1207–17.
[9] Wei D, Lu X, Lu Z, Gu J. Performance analysis and optimization of organic Rankine cycle (ORC) for waste heat recovery. Energy Convers Manage 2007;48:1113–9.
[10] Wei D, Lu X, Lu Z, Gu J. Dynamic modeling and simulation of an organic Rankine cycle (ORC) for waste heat recovery. Appl Therm Eng 2008;28:1216–24.
[11] Dynasim AB. Dynamic modeling laboratory. http://www.dymola.com/.
[12] Drescher U, Bruggemann D. Fluid selection for the organic Rankine cycle (ORC) in biomass power and heat plants. Appl Therm Eng 2007;27:223–8.
[13] Mago PJ, Chamra LM, Srinivasan K, Somayaji C. An examination of regenerative organic Rankine cycles using dry fluids. Appl Therm Eng 2008;28:998–1007.
[14] Lemort V, Quoilin S, Cuevas C, Lebrun J. Testing and modeling a scroll expander integrated into an organic Rankine cycle. Appl Therm Eng 2009;29:3094–102.
[15] Dai Y, Wang J, Gao L. Parametric optimization and comparative study of organic Rankine cycle (ORC) for low grade waste heat recovery. Energy Convers Manage 2009;50:576–82.
[16] Angelino G, Colonna di Paliano P. Multicomponent working fluids for organic Rankine cycles (ORCs). Energy 1998;23:449–63.
[17] Chen Y, Lundqvist P, Johansson A, Platell P. A comparative study of the carbon dioxide transcritical power cycle compared with an organic Rankine cycle with R123 as working fluid in waste heat recovery. Appl Therm Eng 2006;26:2142–7.
[18] Diego AA, Timothy AS, Ryan KJ. Theoretical analysis of waste heat recovery from an internal combustion engine in a hybrid vehicle. SAE 2006-01-1605.
[19] Teng H, Regner G, Cowland C. Waste heat recovery of heavy-duty diesel engines by organic Rankine cycle part I: hybrid energy system of diesel and Rankine engines. SAE 2007-01-0537.
[20] Teng H, Regner G, Cowland C. Waste heat recovery of heavy-duty diesel engines by organic Rankine cycle part II: working fluids for WHR-ORC. SAE 2007-01-0543.
[21] Ringler J, Serfert M, Guyotot V, Hubner W. Rankine cycle for waste heat recovery of IC engines. SAE 2009-01-0174.
[22] Atan R. Heat recovery equipment (Generator) in an automobile for an absorption air-conditioning system. SAE 980062.
[23] He W, Wu YT, Ma CF, Ma GY. Performance study on three-stage power system of compressed air vehicle based on single screw expander. Sci China Tech Sci 2010;53:2299–303.
[24] Wall G. Exergy – a useful concept. http://exergy.se/goran/thesis.
[25] Wark K, Richards DE. Thermodynamics. 6th ed. Singapore: McGraw-Hill; 1999.
[26] Cengel YA, Boles MA. Thermodynamics – an engineering approach. 6th ed. London: McGraw-Hill; 2008.
[27] Liu GY, Liu XD, Qian LL, Yuan Y. Engineering thermodynamics. 2nd ed. Beijing: Higher Education Press; 1989.
[28] Yari M. Performance analysis of the different organic Rankine cycles (ORCs) using dry fluids. Int J Exergy 2009;6:323–42.
[29] Wang EH, Zhang HG, Fan BY, Liang H, Ouyang MG. Study of gasoline engine waste heat recovery by organic Rankine cycle. In: Proceedings of 2010 international conference on electrical engineering and automatic control, 2010 Nov 26–28, Zibo, China, vol. 12. IEEE; 2010. p. 44–8.
[30] Heywood JB. Internal combustion engine fundamentals. New York: McGraw-Hill; 1998.
[31] Liu LD. Research on the single screw expander and organic Rankine cycle system [Dissertation]. Beijing: Beijing University of Technology; 2010.
[32] MATLAB version R14SP3, Matlab help. US: the MathWorks, Inc.; 2005.
[33] REFPROP version 7.1, NIST standard reference database 23. America: the U.S. Secretary of Commerce; 2003.
[34] Poling BE, Prausnitz JM, O'Connell JP. The properties of gases and liquids. 5th ed. New York: McGraw-Hill; 2001.
[35] David R. Handbook of chemistry and physics. 80th ed. Boca Raton: CRC Press; 1999.
[36] Badr O, O'Callaghan PW, Probert SD. Thermodynamic and thermophysical properties of organic working fluids for Rankine-cycle engines. Appl Energy 1985;19:1–40.